Paper pa02-081
Submitted to the 28th International Conference on High Energy Physics
ICHEP'96, Warsaw, Poland, July 1996

Comparison of Charged Particle Pseudorapidity Distributions in Real and Virtual Photon–Proton Collisions

H1 Collaboration

Abstract

Using data taken at the HERA ep collider, measurements are presented of the dependence on pseudo-rapidity in the photon-proton CMS of inclusive charged particle production for real (γp, $Q^2 = 0\,\mathrm{GeV}^2$) and virtual ($\gamma^* p$, $8 < Q^2 < 30\,\mathrm{GeV}^2$) photon-proton interactions. A comparison is made for an interval of collision energy W between $150\,\mathrm{GeV}$ and $210\,\mathrm{GeV}$ ($0.3 < y < 0.5$). The results are discussed in terms of a Regge model with screening corrections.

1 Introduction

The measurements of the proton structure function $F_2(Q^2, x)$ in deep–inelastic scattering (DIS) at HERA by the H1 [1] and ZEUS [2] collaborations have revealed a rapid rise of F_2 with decreasing Bjorken–x. These measurements imply a similar rise of the total virtual photon-proton cross section σ_{tot} with increasing interaction energy W which can be parametrised by a simple power-low formula $\sigma_{tot} \propto W^{2\cdot\lambda}$, where λ parametrises the rate, that is derivative, of the rise of the cross section. The value of λ which is found for virtual photon-proton scattering at HERA is significantly larger than that measured in hadron-hadron and real photon collisions [3, 4]. The observed change in the cross section behaviour is a result of the change of the underlying dynamics of the strong interaction. This phenomenon is associated with a transition from a non-perturbative "soft" to a perturbative "hard" regime and is far from being understood within the framework of perturbative Quantum Chromodynamics (pQCD).

Recently, this problem has been addressed by Capella *et al* [5] (CKMT model) within a framework of Reggeon Field Theory (RFT), where high energy particle interaction is described by Pomeron exchange and the slope λ is related to the Pomeron trajectory intercept. At high energy, when the total interaction cross section described by one-Pomeron exchange σ^1_{tot} is large the unitarity correction becomes important and reduces the cross section value

$$\sigma_{tot} = \sigma^1_{tot} - \sigma_{corr} \tag{1}$$

It was shown [6] the unitarity corrections to single Pomeron exchange significantly reduce the value of λ. In the CKMT model the relative contribution of the unitarity corrections decreases quite rapidly when photon virtuality Q^2 increases. Therefore, the value of λ rises with Q^2 as observed experimentally.

In RFT, unitarity corrections to one Pomeron exchange diagram are approximated by multiple Pomeron exchange. The presence of the latter modifies the properties of the hadronic final state. This mechanism implies the splitting of each colliding particles into several particles moving almost in parallel before the collision. The final state appears as a result of interaction of pairs of such secondaries. In this picture two new different event topologies arise: diffractive particle production with large rapidity gaps and low multiplicity and events with very high particle density, where several pairs of secondaries produce showers. The relative contributions of these different event topologies are predicted by the AGK cutting rules [7]. The remarkable property of the AGK prediction is a cancelation of the unitarity correction contributions in the inclusive particle cross section $(d\sigma_{ch}/d\eta)$ in the central rapidity region

$$\frac{d\sigma_{ch}}{d\eta} = \sigma^1_{tot} \cdot \frac{dN^1_{ch}}{d\eta}, \tag{2}$$

where $(dN^1_{ch}/d\eta)$ is charged particle density resulted from one Pomeron exchange. According to (2) the energy behaviour of the inclusive particle cross section around $\eta = 0$ is defined by the energy behaviour of unscreened one Pomeron exchange and is universal in all interactions. The multi-Pomeron contribution, however, influences the multiplicity fluctuations and defines a behaviour of a second and higher moments of multiplicity spectra.

Although the AGK rules are derived for asymptotically high energies, this theoretical approach proved to be powerful in predicting of non-trivial phenomena in high energy hadronic collisions like the rise of rapidity plateau with energy, violation of the KNO scaling, long range particle-particle correlations etc. The comprehensive review on this subject can be found elsewhere [8]. Thus, the explanation of the change in energy behaviour with photon virtuality within CKMT model leads to the definite predictions about hadronic final state.

Therefore, along with the inclusive cross section measurement, studies of hadronic final state properties as a function of the photon virtuality at HERA provide important information on the dynamics of the strong interaction beyond the domain of validity of perturbative calculations. In this paper we present measurements of charged particle density as function of pseudorapidity in the photon-proton rest frame both in photoproduction and in virtual photon-proton collisions. A comparison of the two data samples is discussed within the framework of the above theoretical approach.

2 Detector Description and Selection of the Events

A detailed description of the H1 apparatus can be found elsewhere [9]. The following describes briefly the components of the detector relevant for this analysis, which makes use of the Backward Electromagnetic Calorimeter (BEMC), the luminosity system and the central tracking detector.

The BEMC (depth of 22.5 radiation lengths or 1 interaction length) covers the backward region of the detector, $151 < \theta < 177°$. The polar angle θ is defined with respect to the proton beam direction ($+z$ axis). A major task of the BEMC is to trigger on and measure the scattered positrons in DIS processes with Q^2 values ranging from 5 to $100\,\mathrm{GeV}^2$. The BEMC energy scale for positrons is known to an accuracy of 1.7%.

A small angle detector (positron tagger), which is part of the luminosity system, is a TlCl/TlBr crystal calorimeter with an energy resolution $\sigma_E/E = 0.1/\sqrt{E\,[\mathrm{GeV}]}$. It is located at $z = -33$ m and accepts positrons from photoproduction processes with an energy fraction between 0.2 and 0.8 with respect to the positron beam energy. The angular acceptance of the positron tagger is restricted to the range $\theta' < 5$ mrad ($\theta' = \pi - \theta$).

Charged particle tracks are measured in two concentric "jet" drift chamber modules (CT), covering the polar angular range $15 < \theta < 165°$. The drift chamber is interleaved with an inner and an outer double layer of multi-wire proportional chambers (MWPC), which were used for the trigger to select events with charged tracks pointing to the interaction region. A superconducting solenoid provides a uniform magnetic field of 1.15 T parallel to the beam axis in the tracking region.

The events used in this analysis were taken during the 1994 running period, in which $27.5\,\mathrm{GeV}$ positrons on $820\,\mathrm{GeV}$ protons were in collision in HERA, and they correspond to an integrated luminosity of $1.5\,\mathrm{pb}^{-1}$. The photoproduction events are triggered by a coincidence of an energy deposit in the small angle positron detector and at least one track pointing to the interaction region. The track condition is derived from the cylindrical MWPC and requires a $p_T \gtrsim 200\,\mathrm{MeV}/c$. This trigger was downcaled during the run such that an effective integrated luminocity for the photoproduction event sample corresponds to about $65\,\mathrm{nb}^{-1}$. The DIS sample consists of events where the scattered positron is detected in the BEMC. The events are triggered by requiring a cluster of more than 4 GeV in the BEMC. Further details of the scattered positron identification procedure in the BEMC and in the small angle positron detector can be found in [1] and [4] respectively. In both event samples the z position of the event vertex reconstructed from charged tracks was required to be within ± 25 cm of the nominal interaction point.

The kinematic variables Q^2 and y of the ep collision are determined from the scattered positron using the following: $Q^2 = 4\,E_e\,E'_e\cos^2(\theta_e/2)$ and $y = 1 - (E'_e/E_e)\cdot\sin^2(\theta_e/2)$, where E_e is the energy of the incident positron and E'_e and θ_e are the energy and the polar angle of the scattered positron respectively. The variable y represents the fraction of the energy of the positron transferred to the proton in the proton rest frame. In the photoproduction sample Q^2 is restricted by the angular acceptance of the positron tagger to be $< 10^{-2}\,\mathrm{GeV}^2$, whilst in the DIS sample we require $8 < Q^2 < 30\,\mathrm{GeV}^2$. For both data samples a limited range energy of photon-proton collision (W) is chosen for comparison by requiring $0.3 < y < 0.5$ with average $\overline{W} \approx 190\ GeV$. The selected data samples contain about $4.3\cdot 10^3$ and $1.1\cdot 10^3$ events for photoproduction and DIS correspondingly.

The data are corrected for detector effects using samples of Monte Carlo (MC) generated events which were fully simulated in the H1 detector. The PHOJET [10] generator for photoproduction and the CDM [11] (Colour Dipole Model) generator for DIS processes were used. In addition a diffractive dissociation contribution in DIS was simulated using the RAPGAP event generator [12]. These particular MC models are chosen as they provide the best description of the hadronic final states in photon-proton collisions. The influence of the QED radiative corrections for the DIS sample was estimated by using the HERACLES program [13].

3 Results and discussion

For comparisons of event properties in both event samples, the $\gamma^* p$ center of mass system (CMS) is chosen as the frame of reference. The measured momenta of charged particles were rotated into the CMS frame by Lorenz transformation assuming a pion mass for all charged tracks. The charged particle density is obtained in terms of the rapidity of each produced particle, which can be approximated by the pseudorapidity $\eta = \ln(\tan(\theta^*/2))$ in the CMS. Here θ^* is the polar angle of a particle in the CMS frame with respect to the proton direction.

The result for charged particle density depends on the event category which is selected for the averaging. Below we present results for two following event categories.

- All photon-proton collision events with more then one hadron in the final state (the "total" event sample).
- A "non-diffractive" event sample, defined by the requirement of at least one particle originating directly from the interaction vertex within the central rapidity interval $-1.0 < \eta < 1.0$. This event sample does not contain low mass diffractive dissociation and quasi–elastic vector meson production events. These two types of events were purposely excluded from the comparison of photoproduction and DIS data as their

relative contribution to the total photon-proton cross section changes rapidly with Q^2.

The results for the charged particle density in the non-diffractive event samples were obtained with data sub-samples where the additional requirement of at least 0.5 GeV energy detected in the calorimeter within $4 < \theta < 15°$ was made. This requirement has high efficiency for the non-diffractive events and removes explicitly the contribution from both low mass diffractive dissociation and quasi-elastic vector meson production.

An interval of $0.5 < \eta < 3.5$ is used for the measurement, where the correction for track reconstruction efficiency is small. A correction as function of η was calculated using MC simulation and applied to the measured particle pseudorapidity distributions. This correction takes into account the track losses due to detector acceptance and to the event selection efficiency. The latter part of the correction depends on the event topology and is largest for the photoproduction total event sample, where about 19% of events (mainly low mass diffractive dissociation and quasi-elastic vector meson production) have no charged tracks within the central track chamber and do not pass the trigger and selection conditions. The uncertainty from the different event topology contributions is estimated using the recent H1 measurement of the photoproduction cross section decomposition [4]. This uncertainty is small in the DIS event sample. The track reconstruction efficiency calculation was cross checked by a visual scan of events. The track efficiency is close to 100% in the central part of the rapidity interval and decreases to about 80% at the edges of the interval due to geometrical acceptance of the drift chamber. The influence of the geometrical acceptance has been checked with photoproduction data by changing the y range. The contribution of decay products from secondary K^0_S and Λ decays is subtracted, and a correction made.

The corrected charged particle pseudorapidity distributions in photoproduction and DIS are shown in Fig. 1 for the total and the non-diffractive event samples. The statistical errors only are shown in the Fig. 1. The systematic errors are dominated by the following uncertainties: track reconstruction and vertex fit efficiency ($\pm 2\%$ with additional -6% for the lowest η bin where the correction is largest), the track trigger condition in the photoproduction sample ($\pm 2\%$), residual background contamination in the photoproduction sample ($\pm 2\%$), K^0_S and Λ subtraction ($\pm 1\%$), losses of events with low charged particle multiplicity in the total photoproduction event sample ($\pm 6\%$), and a correction for the contamination of diffractive events in the non-diffractive sub-sample ($\pm 1\%$).

The charged particle density for non-diffractive events (Fig.1a) is very similar to DIS and photoproduction data for $\eta > 1.5$. This observation is non-trivial from the point of view that the production of final state hadrons is initiated by a "hard" process in DIS which is not present in photoproduction. This surprising finding supports the recent H1 measurement of average charged multiplicity in the photon hemisphere of non-diffractive DIS event [14]. In [14] no significant variation with Q^2 was observed for the both mean value and width of charged particle multiplicity distribution in the range $10 < Q^2 < 1000\ GeV^2$ for fixed interval of W. In the Fig.1 close to the central rapidity region the photoproduction data show a higher multiplicity than the DIS data. This observation qualitively supports the AGK picture, where the central rapidity particle density in non-diffractive events is proportional to an average number of cut Pomerons contributing to the inclusive cross section. This number is larger in photoproduction.

The major difference in the charged particle production rate between DIS and real photon-proton collision is related to a difference in the relative contribution of low multiplicity events (low mass photon diffractive dissociation including vector meson production) in DIS and photoproduction. This difference is clearly visible when the charged particle production rates are normalized to the total cross section (Fig. 1b), where the DIS data points exceed those of photoproduction in the whole rapidity interval with an excess which is least as η tends to 0. In Fig. 1 the difference between particle density in non-diffractive and total event samples is larger for photoproduction than for DIS. This is in agreement with the expectation of larger multiplicity fluctuations in photoproduction discussed above.

In Fig. 2 the photoproduction data are compared with the measurements made by the UA5 collaboration for $p\bar{p}$ collisions at $\sqrt{s} = 200\,\mathrm{GeV}$ [15]. The UA5 inelastic data are shown scaled down by 18% to take into account the elastic $p\bar{p}$ scattering cross section [16]. For comparison with non-diffractive photoproduction data we used so-called non-single diffractive $p\bar{p}$ data. In the fragmentation region the protons show somewhat shrinked pseudorapidity distribution than in γp collisions. This fact can be explained by different distribution of the constituent quark momentum within the photon and proton. The difference in the shape in the central rapidity region (dip in the UA5 data) is related to the mass effect in the Lorenz transformation. It is interesting to note that the particle density around the central rapidity interval ($\eta \gtrsim 1$) is similar for γp and $p\bar{p}$ interactions in both the non-diffractive and the total samples. Thus the observation of similarity of the transverse energy distributions in the central region of pseudorapidity for real photon–hadron and hadron–hadron collisions [17] is also found to be the case for the particle density distributions. This adds weight to the hypothesis of the universality of strong interaction dynamics in the central collision region irrespective of the specific nature of the interacting particles. In the spirit of the CKMT approach, this universal behaviour of the central plateau is closely related to the observed universal energy behaviour of hadron-hadron and real photon-proton collisions at high energy.

On Fig. 3 the energy W dependence of the central charged particle density $\rho(0)$ for the total cross section is shown.

$$\rho(0) = \frac{1}{\sigma_{tot}} \frac{d\sigma_{ch}}{d\eta} \; . \tag{3}$$

In Fig. 3 the H1 data are presented together with low energy DIS [18], pp [19, 20] and high energy $p\bar{p}$ [15] measurements. The H1 values of $\rho(0)$ are obtained by extrapolation from the measured η interval. An estimate of the extrapolation error is included into systematic uncertainty shown in the Fig. 3. The proton collision data are corrected for the elastic cross section. The $\rho(0)$ steeply rises with W in the proton collisions. The DIS data show, however, less energy dependence. This difference is expected from the AGK expression (2) and simply shows difference in the energy behaviour of the unscreened (one Pomeron σ^1) and the total cross sections. The fast energy rise of the virtual photon cross section impies a slow increase of the central particle density in DIS with energy. The latter is valid only if the bare (unscreened) Pomeron has universal properties for both the energy behaviour and final state hadron production independent on the type of collision. This hypothesis of the Pomeron universality is supported by comparison shown in the

Fig.3.

4 Summary

A measurement of charged particle density has been obtained in terms of the pseudorapidity of produced particles in the photon–proton center of mass system for photoproduction and DIS events at the same collision energy. The measurement is presented for a pseudorapidity interval of $0.5 < \eta < 3.5$. The comparison of the two data samples shows that for non–diffractive events charged particle density is surprisingly similar for DIS and photoproduction with slightly higher value for photoproduction in the central rapidity region $\eta < 1.5$. For the total event sample the charged particle density in DIS is larger than in photoproduction in the whole rapidity interval with a tendency to have closer values towards the $\eta = 0$. The H1 measurements of central particle density ($\rho(0)$) are compared with available hadronic collision data at different collision energies. The observation of $\rho(0)$ weak energy dependence in DIS supports the hypothesis of the Pomeron universality in high energy scattering with differences seen in the cross section behaviour and final state hadron production attributed to the different contribution of the unitarity corrections.

Acknowledgments

We are grateful to the HERA machine group whose outstanding efforts have made and continue to make this experiment possible. We thank the engineers and technicians for their work in constructing and now maintaining the H1 detector, our funding agencies for financial support, the DESY technical staff for continual assistance, and the DESY directorate for the hospitality which they extend to the non–DESY members of the collaboration. We thank further M.G.Ryskin, A.B.Kaidalov and R.Engel for useful discussions.

References

[1] H1 Collab., T.Ahmed et al., Nucl. Phys. B439 (1995) 471.

[2] ZEUS Collab., M.Derrick et al., Z. Phys. C65 (1995) 379.

[3] A.Donnachie and P.V.Landshoff, Phys. Lett. B296 (1992) 227.

[4] H1 Collab., S.Aid et al., Z. Phys. C69 (1995) 27.

[5] A.Capella, A.Kaidalov, C.Merino and J.Tran Thanh Van, Phys. Lett. B337 (1994) 358.

[6] A.B.Kaidalov, L.A.Ponomarev and K.A.Ter-Martirosyan, Sov. J. Nucl. Phys. 44 (1986) 468.

[7] V.Abramovskii, V.N.Gribov and O.V.Kancheli, Sov. J. Nucl. Phys. 18 (1974) 308.

[8] A.Capella et al., Phys.Rep. 236 (1994) 227.

[9] H1 Collab., I. Abt et al., “The H1 detector at HERA”, DESY preprint 93-103 (1993)

[10] R.Engel, Proceedings of the XXXIXth Rencontre de Moriond, ed. J.Tran Thanh Van, (edition frontieres, 1994) 321.

[11] L.Lönnblad, Computer Phys. Comm. 71 (1992) 15.

[12] H1 Collab., T. Ahmed et al., Nucl. Phys. B429 (1994) 477.

[13] A.Kwiatkowski, H.Spiesberger and H.-J.Möhring, Computer Phys. Comm. 69 (1992) 155.

[14] H1 Collab. S.Aid, et al., “Charged Particle Multiplicities in Deep-Inelastic Scattering at HERA”, to be pablished.

[15] UA5 Collab. G.J.Alner, et al., Z. Phys. C33 (1986) 1.

[16] Particle Data Group, M.Aguilar-Benitez, et al., Phys. Rev. D50 (1994).

[17] H1 Collab. S.Aid, et al., Phys. Lett. B356 (1995) 118.

[18] EMC Collab., M.Arneodo et al., Z. Phys. C35 (1987) 335.

[19] NA22 Collab., M.Adamus et al., Z. Phys. C39 (1988) 311.

[20] W.Thomé et al., Nucl.Phys. B129 (1977) 365.

H1 Preliminary

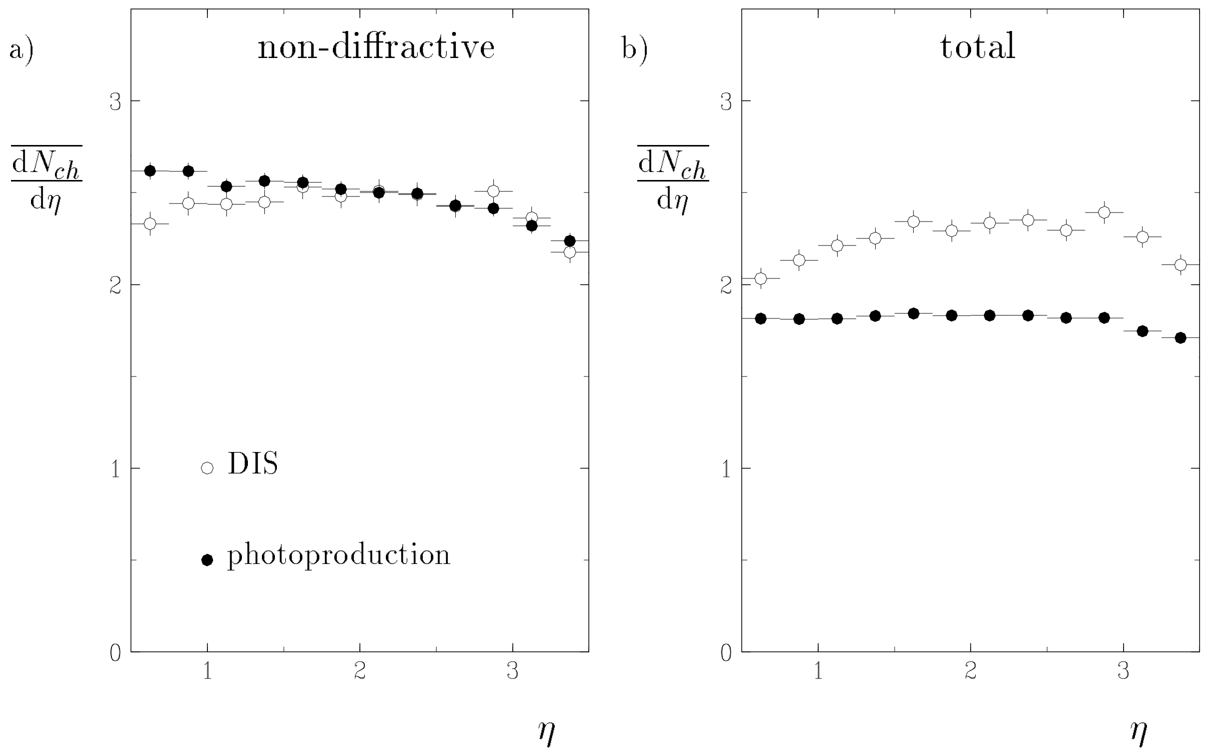

Figure 1: The charged particle pseudorapidity distribution in the hadronic CMS; photoproduction data (full circles) are compared with DIS data ($8 < Q^2 < 30\,\mathrm{GeV}^2$, open circles) in the same y range $0.3 < y < 0.5$ ($\overline{W} = 190\,\mathrm{GeV}$) for the non-diffractive (a) and for the total (b) event samples; only the statistical errors are shown; systematic errors are discussed in the text.

H1 Preliminary

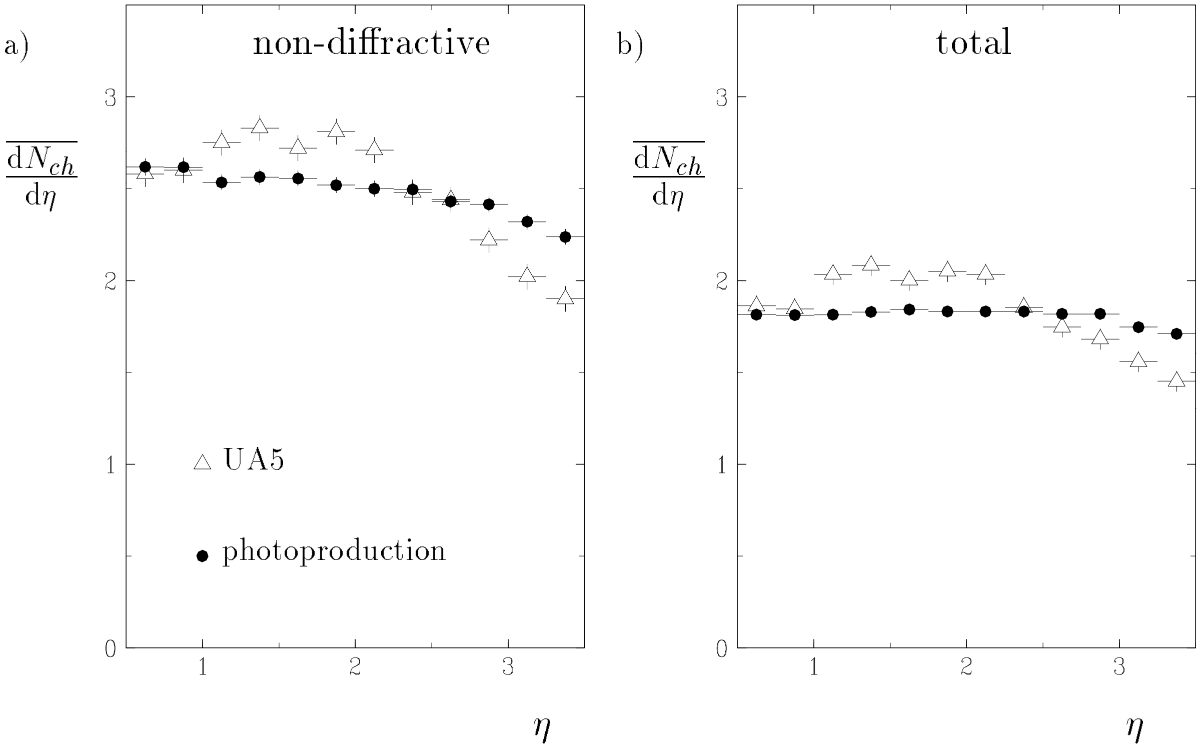

Figure 2: The charged particle pseudorapidity distribution in the hadronic CMS; photoproduction data $\overline{W} = 190\,\mathrm{GeV}$ (full circles) are compared with UA5 data at CMS energy 200 GeV (triangles) for the non-diffractive (a) and the total (b) event samples; for H1 photoproduction data, only the statistical errors are shown; systematic errors are discussed in the text.

H1 Preliminary

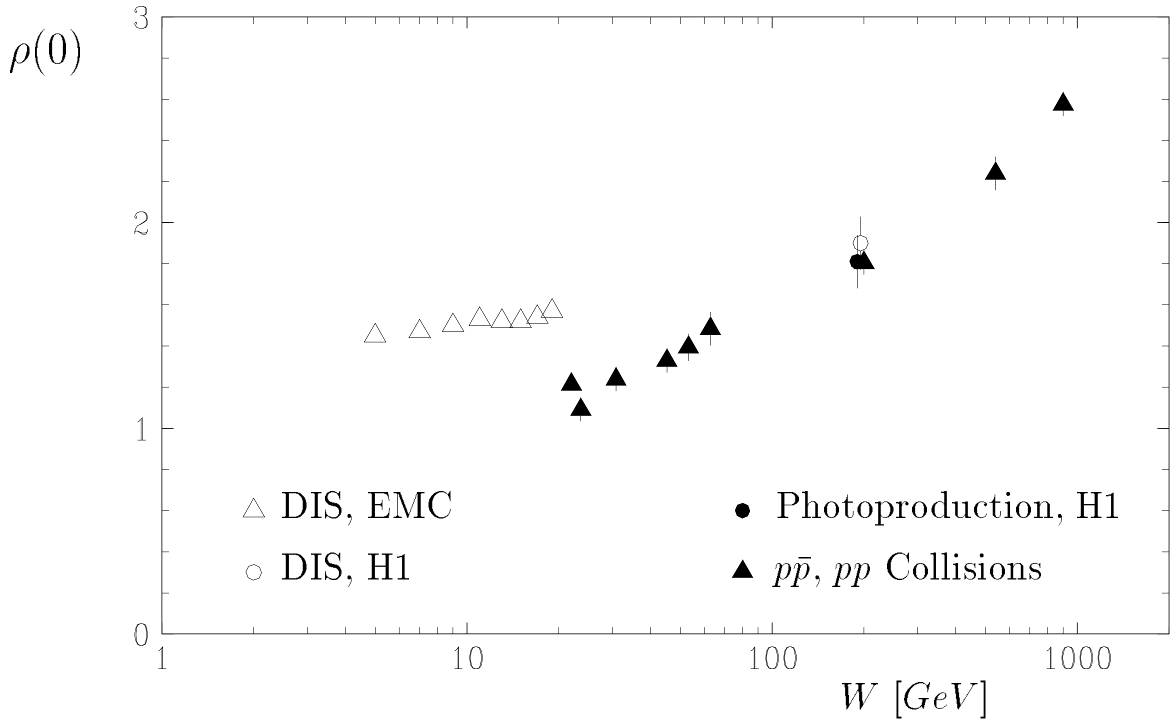

Figure 3: The central charged particle density $\rho(0)$ plotted as function of c.m. energy. The H1 results for photoproduction ($\bullet$) and DIS ($\circ$) compared with data from DIS and proton collisions available at lower and higher energies.